Eur. Phys. J. Special Topics **224**, 3257–3270 (2015)

DOI: 10.1140/epjst/e2015-50101-x

THE EUROPEAN PHYSICAL JOURNAL SPECIAL TOPICS

Regular Article

# Simulation and analysis of a model dinoflagellate predator-prey system

M.J. Mazzoleni[1,a], T. Antonelli[2,b], K.J. Coyne[3,c], and L.F. Rossi[4,d]

[1] Department of Mechanical Engineering and Materials Science, Duke University, Durham NC 27708, USA
[2] Biomathematics Program, Department of Mathematics, North Carolina State University, Raleigh, NC 27695, USA
[3] College of Earth, Ocean, and Environment, University of Delaware, Lewes, DE 19958, USA
[4] Department of Mathematical Sciences, University of Delaware, Newark, DE 19716, USA

Received 15 May 2015 / Received in final form 2 November 2015
Published online 15 December 2015

**Abstract.** This paper analyzes the dynamics of a model dinoflagellate predator-prey system and uses simulations to validate theoretical and experimental studies. A simple model for predator-prey interactions is derived by drawing upon analogies from chemical kinetics. This model is then modified to account for inefficiencies in predation. Simulation results are shown to closely match the model predictions. Additional simulations are then run which are based on experimental observations of predatory dinoflagellate behavior, and this study specifically investigates how the predatory dinoflagellate *Karlodinium veneficum* uses toxins to immobilize its prey and increase its feeding rate. These simulations account for complex dynamics that were not included in the basic models, and the results from these computational simulations closely match the experimentally observed predatory behavior of *K. veneficum* and reinforce the notion that predatory dinoflagellates utilize toxins to increase their feeding rate.

## 1 Introduction

Dinoflagellates are the second largest group of phytoplankton in marine environments [15,29]. They comprise a diverse group of species with lifestyles ranging from symbiotic associations with corals to free-living flagellates to parasitic species [24,28]. Trophic status can also vary, with the number of heterotrophic and autotrophic species about equally divided. There is mounting evidence, however, that the majority of autotrophic dinoflagellate species are also mixotrophs [16,35]: they are capable of growth through photosynthesis but may also acquire carbon through predation. Predatory dinoflagellates, along with other microzooplankton species in the marine environment,

[a] e-mail: michael.mazzoleni@duke.edu
[b] e-mail: tdantone@ncsu.edu
[c] e-mail: kcoyne@udel.edu
[d] e-mail: rossi@math.udel.edu

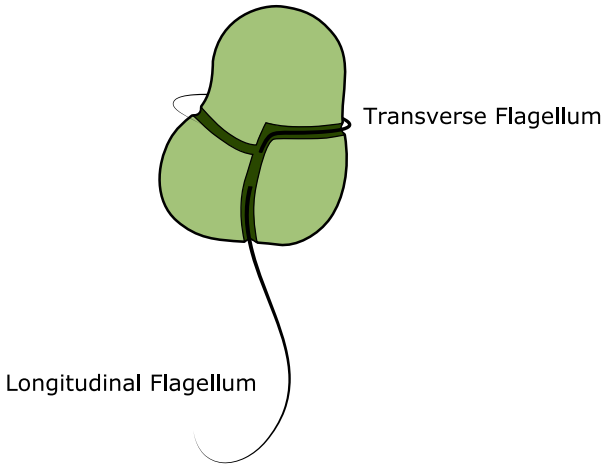


**Fig. 1.** Schematic of a dinoflagellate identifying the two flagella.

consume about 60% of marine primary production [25] and thus are an important avenue for the transfer of carbon to higher trophic levels.

Predation by dinoflagellates and other microzooplankton species is driven by swimming behavior in response to chemical gradients [4,11,19]. Dinoflagellates swim using two flagella, a transverse flagellum and a longitudinal flagellum, that emanate from the ventral side of the cell in most dinoflagellate species (see Fig. 1). The ribbon-like transverse flagellum is located in a groove, the cingulum, which lies around the mid-section of the cell and provides forward locomotion and rotation about the cell's axis. The longitudinal or trailing flagellum also provides forward propulsion and lies in the sulcus, a groove that transverses from the flagellar pore to the posterior end. Differences in the placement of the flagellar groove result in swimming characteristics that differ between species. The combination of logitudinal and transverse flagellar motion results in a helical swimming pattern (see Frenchel for an overview [12]) and allows the cell to orient itself in response to chemical gradients and the presence of prey. For instance, to demonstrate that it is possible for helical swimmers to track up or down a gradient, Crenshaw explored an empirical control strategy that adjusts the orientation of the swimmer's angular momentum based on its instantaneous response to a sensed chemical field [8]. In the first part of this work, we seek to connect the swimming properties of dinoflagellate predators and prey with their grazing success. We characterized the predation rate of dinoflagellates from fundamental physical principles, drawing upon basic ideas of chemical kinetics and known properties of phytoplankton swimming to derive a mathematical model for predation.

A small number of dinoflagellates are also considered harmful algal bloom (HAB) species and produce a suite of complex toxic compounds. The release of toxins during blooms (commonly known as red tides) can impact human health through shellfish poisoning or impact marine ecosystems by causing massive fish kills [13,17,18,31]. Toxin production by HAB dinoflagellates may confer an ecological advantage to these species by inhibiting grazers (e.g. [6,30,34]). Recent studies, however, indicate that toxin production by mixotrophic dinoflagellates may also facilitate predation by immobilizing prey [27]. Here, we describe a set of simulations based on experimental observations of Sheng et al. [26,27] for the mixotrophic dinoflagellate, *Karlodinium veneficum* [5,21,22]. *K. veneficum* is a globally distributed HAB dinoflagellate that produces a potent toxin, karlotoxin (KmTx) [9,10,32,33], that kills fish and contributes to harmful algal bloom formation [2,17]. The effects of KmTx were also

observed to significantly slow down and often immobilize the prey of *K. veneficum* [27], leading Sheng et al. to conclude that toxin production played a role in predation success. Moreover, Sheng et al. also demonstrated that toxic *K. veneficum* dramatically altered its own swimming behavior in the presence of prey. In the second part of this study, we use theory and computational simulations based on our mathematical model for predation to explain experimental observations of Sheng et al. We show that toxin-induced changes in swimming behavior of *K. veneficum* and its prey enhance predation by influencing (i) the frequency of predator-prey encounters and (ii) the efficiency of converting those encounters into successful predation. To our knowledge, this is the first mechanistic model to describe predation rates of *K. veneficum*.

## 2 Determining the rate of predator-prey encounters when predation is perfectly efficient

This section derives a simple relationship for the rate of predator-prey encounters when predation is perfectly efficient by drawing upon analogies from chemical kinetics [3]. A set of simulations is then used to validate this model, with the results showing good agreement between theory and simulation. The parameters used in the simulations were based on experimental observations of dinoflagellate behavior [26,27].

### 2.1 Mathematical model for perfectly efficient predation

Simple mass-action linear behavior between predators (A) and prey (B) is common in nature, and phytoplankton predation is no exception. Thus, if $\rho_A$ and $\rho_B$ denote the densities of the predator and prey species respectively, then

$$\frac{d\rho_B}{dt} = -k\rho_A\rho_B, \tag{1}$$

where $k$ is a constant that is independent of the predator-prey densities which determines the decline in the prey population due to predator-prey encounters. Unfortunately, these models are too general to provide much predictive power to scientists because $k$ must be empirically determined. One of our objectives is to systematically derive and verify how $k$ depends on independently measurable environmental quantities. For predation to occur, predator and prey must first encounter each other. If we assume that these single-celled organisms cannot sense each other at ranges exceeding a body length, then encounters are purely random. Drawing upon basic analogies from chemical kinetics [3], we can derive a simple expression to quantify encounter rates. If we assume the predators and prey are spheres with radii $r_A$ and $r_B$, and that the predator moves at speed $S$ relative to prey, a solitary predator will encounter

$$\pi(r_A + r_B)^2 S\ \Delta t\ \rho_B \tag{2}$$

prey individuals in time $\Delta t$ as shown in Fig. 2. So the encounter rate between predators and prey is

$$\underbrace{\pi(r_A + r_B)^2 S}_{k}\rho_A\rho_B, \tag{3}$$

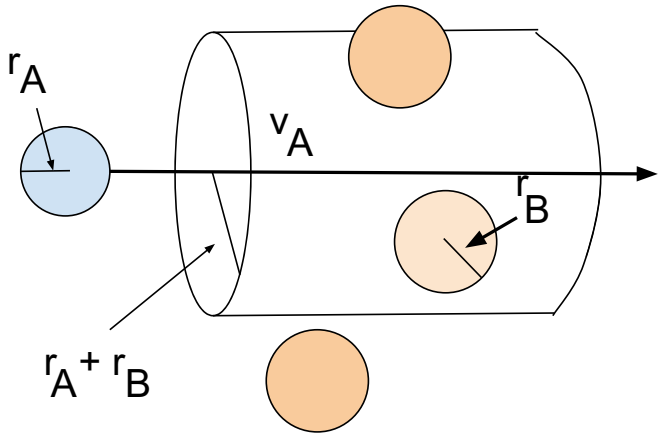


**Fig. 2.** The geometry of predator-prey encounters. A predator will encounter any prey that are within the indicated cylinder surrounding its path.

in agreement with the mass-action assumption commonly used in ecological modeling. To calculate a mean encounter speed, we begin with the law of cosines on $\mathbf{v}_{\rm rel} = \mathbf{v}_A - \mathbf{v}_B$,

$$|\mathbf{v}_{\rm rel}|^2 = |\mathbf{v}_A|^2 + |\mathbf{v}_B|^2 - 2|\mathbf{v}_A||\mathbf{v}_B|\cos\varphi, \tag{4}$$

where $\mathbf{v}_A$ and $\mathbf{v}_B$ are the velocities of the predator and prey individuals, respectively. If we define $\alpha = |\mathbf{v}_A|/|\mathbf{v}_B|$ then

$$|\mathbf{v}_{\rm rel}|^2 = |\mathbf{v}_A||\mathbf{v}_B|\left(\alpha + \alpha^{-1} - 2\cos\varphi\right). \tag{5}$$

Without loss of generality, $\varphi$ is the collision angle in a spherical polar coordinate system centered on the predator with the north pole aligned with its direction of motion. The azimuthal angle $\theta$ plays no role in the relative collision speed. If we assume that directions of motion of predators and prey are uniformly distributed, then we can define the ensemble average relative speed as the mean over all possible $\theta$'s and $\phi$'s over which the collision can occur.

$$\begin{aligned}\langle|\mathbf{v}_{\rm rel}|\rangle &\equiv \left[\frac{\int_0^{2\pi}\int_0^{\pi}|\mathbf{v}_A||\mathbf{v}_B|\left(\alpha+\alpha^{-1}-2\cos\varphi\right)\sin\varphi d\varphi d\theta}{\int_0^{2\pi}\int_0^{\pi}\sin\varphi d\varphi d\theta}\right]^{1/2}\\ &= \left[\frac{1}{2}\int_0^{\pi}|\mathbf{v}_A||\mathbf{v}_B|\left(\alpha+\alpha^{-1}-2\cos\varphi\right)\sin\varphi d\varphi\right]^{1/2}\\ &= \left(|\mathbf{v}_A|^2+|\mathbf{v}_B|^2\right)^{1/2}.\end{aligned} \tag{6}$$

In short, we define the mean encounter speed in the $L_2$ or root mean square sense. Following along with our assumption that the predation rate depends only upon the relative speed or kinetic energy of the encounters between predators and prey, the interactions will be independent of the relative orientations $\theta$ of the colliding bodies. We will retain this assumption for the remainder of this paper. We assume that the probability that predation will occur is related to the physical parameters of the collision. For our purposes, we will disregard the orientation of the collision and focus on the collision speed only:

$$P(\text{predation}) = \eta(|\mathbf{v}_{\rm rel}|), \tag{7}$$

where $\eta$ is a function describing the *efficiency* of the predator. The simplest case is when $\eta(|\mathbf{v}_{\text{rel}}|) = 1$, where predation always occurs perfectly whenever a predator and prey meet. Thus, if all the predators move with speed $|\mathbf{v}_A|$ and prey with speed $|\mathbf{v}_B|$, we can use the encounter rate (3) with $S$ replaced by $\langle|\mathbf{v}_{\text{pred}}|\rangle$ to model the prey consumption as

$$\frac{d\rho_B}{dt} = -\pi(r_A + r_B)^2\sqrt{|\mathbf{v}_A|^2 + |\mathbf{v}_B|^2}\rho_A\rho_B, \tag{8}$$

where $r_A$, $r_B$, $\mathbf{v}_A$ and $\mathbf{v}_B$ are all independently measurable parameters. Therefore, the encouter rate (which is the same as the predation rate when predation is perfectly efficient) can be expressed as

$$k = \pi(r_A + r_B)^2\sqrt{|\mathbf{v}_A|^2 + |\mathbf{v}_B|^2}. \tag{9}$$

### 2.2 Simulations for perfectly efficient predation

A set of numerical simulations were run to validate this simple model for predation. The simulations tracked the motion and interactions of predator-prey dinoflagellates. The dinoflagellates were randomly assigned initial positions and orientations within a cubic volume. At each time step, the algorithm updated the positions of each dinoflagellate and determined whether a predator-prey encounter occurred by calculating the absolute distance between predator-prey dinoflagellates from their coordinates to determine if their separation distance was below the critical collision threshold (the sum of the predator and prey radii: $r_A + r_B$). Periodic boundary conditions were applied to the cubic volume in order to simulate an infinite space and remove boundary effects from the simulations. During the simulations, the dinoflagellates moved within the cubic volume in helical trajectories, which matches their observed motile behavior [7,26,27]. Helical motion can be described parametrically as

$$H(t) = R\left[\cos(\omega t)\hat{i} + \sin(\omega t)\hat{j}\right] + \left(\frac{p\omega t}{2\pi}\right)\hat{k}, \tag{10}$$

where $R$ is the helical radius, $\omega$ is the angular frequency, and $p$ is the helical pitch. The velocity $\mathbf{v}$ of a dinoflagellate can be calculated as

$$\mathbf{v} = \omega\sqrt{R^2 + \left(\frac{p}{2\pi}\right)^2}. \tag{11}$$

It is important to remember that the predation rate $k$ is independent of the predator-prey densities. Any density-dependent effects that might be observed in a simulation would be the result of simulation artifacts. It was therefore important to choose sufficient densities of predator and prey and to run the simulation for an adequate amount of time at an appropriate time step to obtain accurate results. If the density was too sparse, the time duration too short, or the time step too large, then random errors were introduced to the computations due to the simulation mechanics operating in a discrete environment as opposed to a continuum. The simulation results were found to converge on a consistent solution when they considered 100 predator dinoflagellates and 100 prey dinoflagellates in a cubic volume of side length 1 mm and were run for 1000 seconds with a time step of 0.01 seconds. A snapshot of the simulation at a given time step can be seen in Fig. 3.

Four different sets of simulations were run to validate the theoretical predation rate $k$ (9). The predator-prey velocities and radii that were selected were based on experimental data collected by Sheng et al. [26,27]. Four different strains of *K. veneficum* were analyzed as the predators, and *S. major* was analyzed as the prey. At this

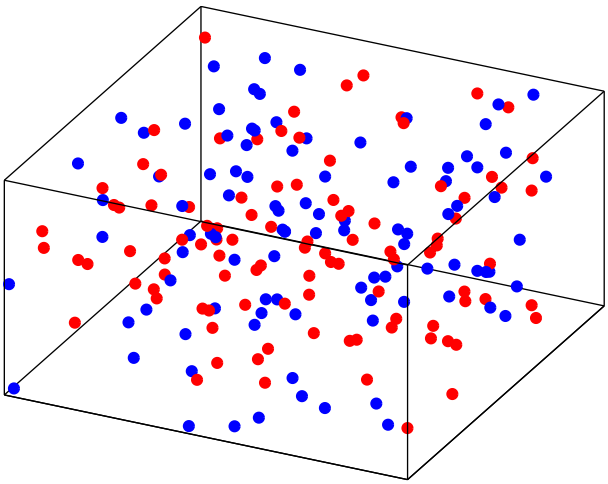

**Fig. 3.** Snapshot of a simulation showing the randomly distributed predators (blue) and prey (red) moving within a cubic volume with periodic boundary conditions.

**Table 1.** Comparison of theoretical and simulated predation rates $k$ when predatory efficiency is assumed to be $\eta = 1$. It should be noted that $r_A = 4.5$ $\mu$m, $r_B = 3.5$ $\mu$m, and $\mathbf{v}_B = 86.4$ $\mu$m/sec for all simulations.

| *K. veneficum* Strain | $\mathbf{v}_A$ ($\mu$m/sec) | Theoretical $k$ (m$^3$/sec) | Simulated $k$ (m$^3$/sec) | % Error |
|---|---|---|---|---|
| MD5 | 81.3 | $2.39 \times 10^{-14}$ | $2.25 \times 10^{-14}$ | 5.9 |
| 1974 | 102.3 | $2.69 \times 10^{-14}$ | $2.54 \times 10^{-14}$ | 5.6 |
| BM1 | 111.2 | $2.83 \times 10^{-14}$ | $2.62 \times 10^{-14}$ | 7.4 |
| 2064 | 80.9 | $2.38 \times 10^{-14}$ | $2.18 \times 10^{-14}$ | 8.4 |

stage of the paper, we are not yet attempting to match experimental results, but are rather trying to validate our theoretical and computational models of predator-prey dinoflagellate dynamics. Therefore, the parameters selected for the simulations were based on the controlled observations where the predator-prey dinoflaggelates were not mixed with each other. One hundred simulations were run for each of the four parameter combinations to provide a large sample size of computational data. The simulated values for $k$ were very close to the theoretical values, with less than 10% error, defined as $|k_{\text{sim}} - k_{\text{th}}|/k_{\text{th}} \times 100\%$ for all cases. The predation rates from simulations are slightly lower than the theoretical values, which is a consistent trend for all cases. This is likely caused by the discrete nature of the simulations, which differs from the continuum that the theory represents. Since the simulations can only analyze positions at discrete times, it is likely that a small number of predator-prey interactions occurred between discrete steps and thus were not counted. This would lead to a slightly lower predation rate for the simulated system. These results are shown in Table 1.

## 3 Accounting for inefficiencies in predation

Not every encounter between a predatory dinoflagellate and its prey results in a successful feeding event. When initial contact is made, the two organisms typically struggle against each other for up to 30 seconds, with the prey often escaping [1]. Some

strains of *K. veneficum* are known to release toxins, which impair the ability of their prey to escape capture and thus increase predation efficiency [1,27]. *K. veneficum* has also been observed to alter its swimming behavior in the presence of prey, typically decreasing its speed. It has been hypothesized that *K. veneficum* does this to to reduce its hydrodynamic profile and thus avoid detection by its prey [26,27]. Therefore, this section modifies the previously derived encounter/predation rate (9) to account for imperfect predator efficiency. We first propose a model that bases the efficiency on a sharp cutoff related to the relative velocities of the predator and prey during their collisions. Simulations are then used to verify this model. A more sophisticated efficiency model based on the individual velocities of the predator and the prey is then presented. This more sophisticated model is applied to computational simulations in Sect. 4 in an attempt to match experimental data.

### 3.1 Mathematical model for inefficient predation based on relative velocity

Realistically, predation will not be perfectly efficient. To explore this further, we define $\mathbf{v}_{\text{pred}}$ to be $\mathbf{v}_{\text{rel}}$ only when predation occurs. In the general case when $\eta(|\mathbf{v}_{\text{rel}}|) \neq 1$, we can calculate $\langle|\mathbf{v}_{\text{pred}}|\rangle$ directly.

$$\begin{aligned}\langle|\mathbf{v}_{\text{pred}}|\rangle &\equiv \left[\frac{1}{2}\int_0^{\pi} |\mathbf{v}_A||\mathbf{v}_B|\left(\alpha+\alpha^{-1}-2\cos\varphi\right)\right.\\ &\quad\left.\times\,\eta(|\mathbf{v}_A||\mathbf{v}_B|\left(\alpha+\alpha^{-1}-2\cos\varphi\right))\sin\varphi d\varphi\right]^{1/2},\\ \frac{\langle|\mathbf{v}_{\text{pred}}|\rangle}{\sqrt{|\mathbf{v}_A||\mathbf{v}_B|}} &\equiv \left[\frac{1}{2}\int_0^{\pi} \left(\alpha+\alpha^{-1}-2\cos\varphi\right)\right.\\ &\quad\left.\times\,\eta(|\mathbf{v}_A||\mathbf{v}_B|\left(\alpha+\alpha^{-1}-2\cos\varphi\right))\sin\varphi d\varphi\right]^{1/2}. \qquad (12)\end{aligned}$$

Predators typically require some handling of the prey for predation to occur. One simple case might be that predation only occurs if the relative encounter speed is below a threshold handling speed $S_{\text{h}} \leq |\mathbf{v}_A| + |\mathbf{v}_B|$,

$$\eta(|\mathbf{v}_{\text{rel}}|) = \begin{cases} 1, & |\mathbf{v}_{\text{rel}}| < S_{\text{h}}, \\ 0, & \text{otherwise} \end{cases}. \qquad (13)$$

Defining $\beta = S_{\text{h}}^2/(|\mathbf{v}_A||\mathbf{v}_B|)$, we can determine a maximum angle $\varphi_0$ at which predation can occur:

$$\varphi_0 = \arccos w, \quad w = \frac{1}{2}\left(\alpha+\alpha^{-1}-\beta\right). \qquad (14)$$

In this case, the normalized predation speed is

$$\begin{aligned}\frac{\langle|\mathbf{v}_{\text{pred}}|\rangle}{\sqrt{|\mathbf{v}_A||\mathbf{v}_B|}} &= \left[\frac{1}{2}\int_0^{\varphi_0} \left(\alpha+\alpha^{-1}-2\cos\varphi\right)\sin\varphi d\varphi\right]^{1/2},\\ &= \frac{1}{2}\left[(1-w)(\alpha+\alpha^{-1}+\beta-2)\right]^{1/2}. \qquad (15)\end{aligned}$$

From (3), we know that the predation rate is directly proportional to $\langle|\mathbf{v}_{\text{pred}}|\rangle$. Therefore, we can rewrite (15) as

$$\langle|\mathbf{v}_{\text{pred}}|\rangle^2 = \frac{S_{\text{h}}^2}{8}\frac{1}{\beta}\left[\beta^2 - \left(2-(\alpha+\alpha^{-1})\right)^2\right]. \qquad (16)$$

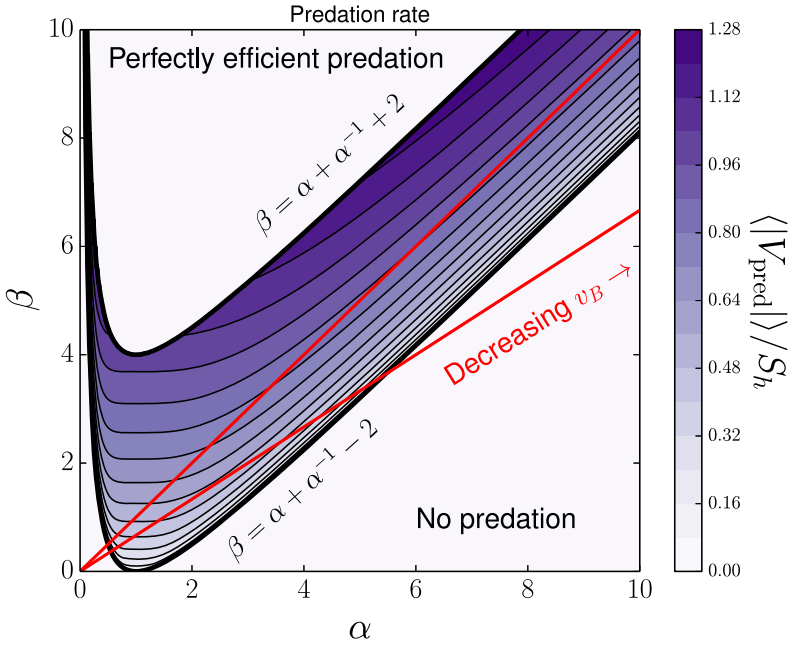


**Fig. 4.** $\langle |\mathbf{v}_{\rm pred}| \rangle / S_{\rm h}$ as a function of $\alpha = |\mathbf{v}_A|/|\mathbf{v}_B|$ and $\beta = S_{\rm h}^2/|\mathbf{v}_A||\mathbf{v}_B|$ over the domain where $S_{\rm h}$ is relevant. The two red lines indicate two level sets of $\mathbf{v}_A$. The lower line has a local maximum within the domain. Note that for the dinoflagellates *K. veneficum* and *S. major*, values of $\alpha$ are typically between 1 and 4. Impairing *S. major* with toxins shifts the position in parameter space up and to the right along lines radiating from the origin.

where this function has the domain $\alpha+\alpha^{-1}-2 \leq \beta \leq \alpha+\alpha^{-1}+2$ from (14). We plot contours of the normalized $\langle |\mathbf{v}_{\rm pred}| \rangle$, which is proportional to the predation rate, over its domain in Fig. 4. A predator-prey system characterized by $\mathbf{v}_A$, $\mathbf{v}_B$ and $S_{\rm h}$ can be visualized as a point $(\alpha, \beta)$ in this contour plot. For $\beta < \alpha + \alpha^{-1} - 2$, predation is impossible because all collision speeds are greater than $S_{\rm h}$, regardless of orientation. This corresponds to a scenario where both predator and prey are moving very quickly relative to the handling threshold, so near perfect alignment in trajectory and speed is necessary for predation to occur. For $\beta > \alpha+\alpha^{-1}+2$, all collisions result in predation:

$$\langle |\mathbf{v}_{\rm pred}| \rangle^2 = \frac{S_{\rm h}^2}{\beta}(\alpha + \alpha^{-1}). \tag{17}$$

We observe that $S_{\rm h}^2\alpha/\beta = |\mathbf{v}_A|^2$ so that in the $(\alpha, \beta)$ plane, level sets of $|\mathbf{v}_A|$ are lines radiating from the origin. (Similarly, levels sets of $|\mathbf{v}_B|$ are hyperbolas.) In Fig. 4, we see that slowing the prey leads to higher predation rates. Along the first upper line (slope=1), $\langle |\mathbf{v}_{\rm pred}| \rangle$ is monotonically increasing along the level set, so lower prey speeds always lead to greater predation rates. Along the lower level set (slope $= 2/3$), there is a local maximum. Notice that all level sets except those with unit slope will eventually leave the domain where $S_{\rm h}$ becomes relevant. These trends establish a theoretical basis for toxins being advantageous in plankton and other similar predator-prey relationships. Toxins have been observed to slow the predators too [27], so a more detailed quantitative analysis of the relative fitness of toxic versus non-toxic species is more complex and left for future work. For instance, if karlotoxin were to slow predator and prey by the same relative amount, it would correspond to an increase in

$\beta$ with constant $\alpha$, yielding higher $\langle|\mathbf{v}_{\text{pred}}|\rangle$. Differing reductions to $\mathbf{v}_A$ and $\mathbf{v}_B$ would shift the state of the system left or right in Fig. 4.

It is more realistic to create a model where there is a distribution of speeds amongst both predator and prey populations as has been observed in experiments [26,27]. That is, the prey density distribution $\mu_B(s,t)$ depends on prey speed $s$ and time $t$, so that the total prey density at any moment in time is:

$$\rho_B(t) = \int_0^\infty \mu_B(s,t)ds. \tag{18}$$

We assume the predator speed distribution is not dependent on time, $\mu_A \equiv \mu_A(s)$. Furthermore, we assume that the orientations of prey moving at any given speed are uniformly distributed and the same is true for predators. Therefore,

$$\frac{\partial \mu_B}{\partial t}(s,t) = -\int_0^\infty k(s',s)\mu_A(s')\mu_B(s)ds', \tag{19}$$

where $k(s',s)$ is the predation rate between predators moving at speed $s'$ and prey moving at speed $s$. We can calculate this value to be:

$$k(s',s) = \pi(r_A + r_B)^2\langle|\mathbf{v}_{\text{pred}}|\rangle_{(s',s)}, \tag{20}$$

where $\langle|\mathbf{v}_{\text{pred}}|\rangle_{(s',s)}$ is the ensemble predation speed between predators moving at speed $s'$ and prey moving at speed $s$ determined by (12). Thus, we can derive an evolution equation for the prey speed distribution:

$$\mu_B(s,t) = \mu_B(s,0)\exp\left[-\pi(r_A + r_B)^2\int_0^\infty \langle|\mathbf{v}_{\text{pred}}|\rangle_{(s',s)}\mu_A(s')ds't\right]. \tag{21}$$

### 3.2 Simulations for inefficient predation based on relative velocity

Simulations similar to the ones presented in Sect. 2.2 were used to validate the model for predation rates presented in Sect. 3.1 which defined efficiency based on a sharp cutoff determined by relative velocity (13). To compare results, we define a normalized predation rate $\bar{k}$,

$$\bar{k} = \frac{\left[(1-w)(\alpha + \alpha^{-1} + \beta - 2)|\mathbf{v}_A||\mathbf{v}_B|\right]^{1/2}}{2\sqrt{|\mathbf{v}_A|^2 + |\mathbf{v}_B|^2}}, \tag{22}$$

where $\bar{k}$ is the predation rate that accounts for inefficiency normalized by the perfectly efficient predation rate (9). One hundred simulations were run for each of the four parameter combinations (see Sect. 2.2), and the cutoff velocity $S_h$ was varied at intervals from zero to the maximum possible relative velocity $(\mathbf{v}_A + \mathbf{v}_B)$. The results can be seen in Fig. 5, which shows close correspondence between the simulated results and the theoretically predicted rates. The rates from simulations are slightly lower than the theoretical values, which is consistent with the simulation results from Sect. 2.2 and likely has similar causes.

### 3.3 Determining predation efficiency by considering predator-prey velocities individually

The simple efficiency model presented in Sect. 3.1 is useful from an illustrative standpoint to demonstrate a basic mechanism to account for predation inefficiency. However, in this section we propose a more sophisticated and phenomenologically accurate

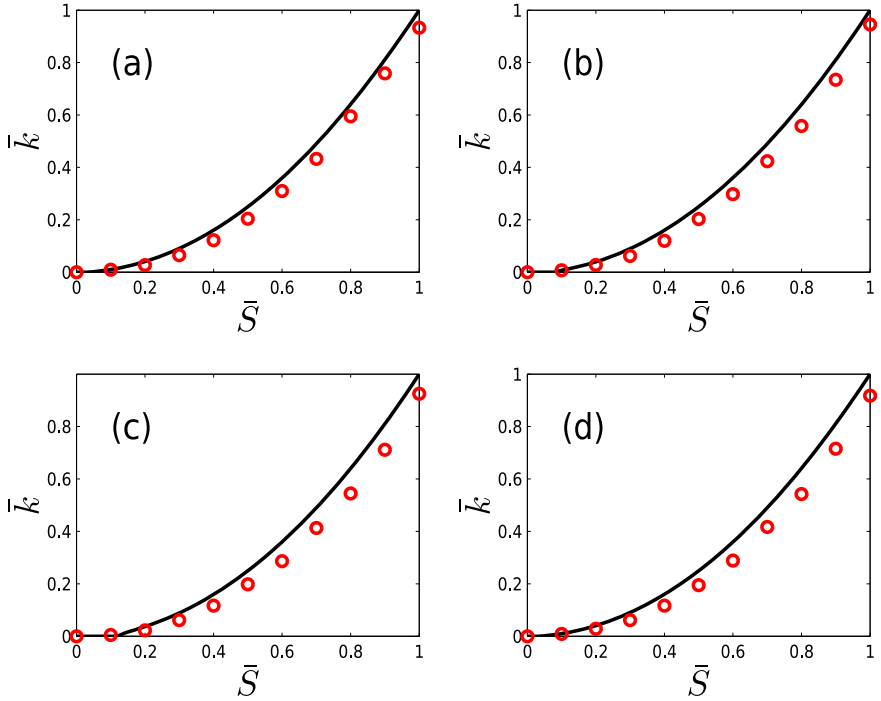


**Fig. 5.** Plots comparing theoretical predation rates to simulated predation rates (22). The black lines represent the theoretical rates, while the red dots represent simulated results. The cutoff velocity has been normalized using the following convention: $\bar{S} = S_h/(\mathbf{v}_A + \mathbf{v}_B)$. The *K. veneficum* strains that were analyzed in the simulations were: (a) MD5, (b) 1974, (c) BM1, and (d) 2064.

efficiency model that accounts for the predator-prey velocities individually. Specifically, we propose a 2-D low-pass filter concept, where the efficiency $\eta$ is given as

$$\eta(\mathbf{v}_A, \mathbf{v}_B) = \frac{1}{\sqrt{1 + \left(\frac{\mathbf{v}_A}{\lambda_A}\right)^{2\xi_A} + \left(\frac{\mathbf{v}_B}{\lambda_B}\right)^{2\xi_B}}}. \tag{23}$$

This "filter" increases the likelihood of successful feeding during a collision when the velocities of both predatory dinoflagellates and their prey are low relative to the cutoff velocities $\lambda_A$ and $\lambda_B$, respectively. The parameters $\xi_A$ and $\xi_B$ are related to the sharpness of the cutoff. This efficiency model is supported by experimental observations of dinoflagellate predation events [1,27]. This 2-D filter model will be implemented with simulations in Sect. 4 to match experimental studies and to gain further insight into the predatory behavior of dinoflagellates.

## 4 Comparisons with experimental studies

This section describes a set of simulations that seek to replicate the experimental results obtained by Sheng et al., who observed that some strains of the mixotrophic dinoflagellate *K. veneficum* release karlotoxins to immobilize their prey and enhance predation [27]. The simulations accounted for the distributed parameters and immotility fractions of the dinoflagellates and calculated predation inefficiencies as a function

**Table 2.** Summary of experimental results from Sheng et al. [27]. Not to be confused with the helical radius $R$, the spherical radii $r_A$ and $r_B$ were 4.5 $\mu$m and 3.5 $\mu$m, respectively, for all cases. Note: the h5 data for experiments involving 1974 is not available.

| Species | $\mathbf{v}$ ($\mu$m/sec) | $R$ ($\mu$m) | $\omega$ (rad/sec) | $\chi$ (%) | $\gamma$ (1/hr) |
|---|---|---|---|---|---|
| S. major (control) | $86.4 \pm 47.0$ | $5.8 \pm 6.1$ | $7.3 \pm 4.0$ | 31 | |
| MD5 (control) | $81.3 \pm 44.9$ | $4.57 \pm 4.9$ | $6.98 \pm 3.7$ | 26 | |
| MD5 (h0) | $84.5 \pm 48.6$ | $4.6 \pm 5.3$ | $6.9 \pm 2.2$ | 25 | |
| MD5 (h5) | $82.3 \pm 50.1$ | $4.7 \pm 5.1$ | $6.8 \pm 3.0$ | 26 | |
| S. major (h0) | $85.2 \pm 46.1$ | $5.1 \pm 5.9$ | $7.2 \pm 3.8$ | 28 | |
| S. major (h5) | $86.8 \pm 40.1$ | $6.1 \pm 4.8$ | $7.8 \pm 2.5$ | 29 | $0.03 \pm 0.12$ |
| 1974 (control) | $102.3 \pm 56.4$ | $9.2 \pm 8.6$ | $5.67 \pm 2.9$ | 17 | |
| 1974 (h0) | $160.4 \pm 59.6$ | $16.2 \pm 5.7$ | $8.7 \pm 6.1$ | 28 | |
| S. major (h0) | $42.7 \pm 37.7$ | $2.9 \pm 4.3$ | $8.1 \pm 4.1$ | 53 | $0.39 \pm 0.13$ |
| BM1 (control) | $111.2 \pm 55.15$ | $9.3 \pm 8.8$ | $6.7 \pm 3.1$ | 6 | |
| BM1 (h0) | $81.8 \pm 55.5$ | $6.5 \pm 7.4$ | $6.4 \pm 3.0$ | 21 | |
| BM1 (h5) | $92.7 \pm 43.6$ | $8.7 \pm 7.5$ | $5.6 \pm 2.7$ | 40 | |
| S. major (h0) | $65.1 \pm 41.9$ | $4.1 \pm 4.8$ | $6.9 \pm 3.2$ | 28 | |
| S. major (h5) | $69.8 \pm 44.6$ | $5.1 \pm 6.0$ | $6.7 \pm 3.3$ | 53 | $0.36 \pm 0.06$ |
| 2064 (control) | $80.9 \pm 38.9$ | $6.5 \pm 6.8$ | $5.0 \pm 2.7$ | 11 | |
| 2064 (h0) | $37.8 \pm 40.1$ | $3.76 \pm 5.0$ | $6.8 \pm 3.8$ | 25 | |
| 2064 (h5) | $59.4 \pm 35.1$ | $4.7 \pm 5.1$ | $5.5 \pm 3.0$ | 25 | |
| S. major (h0) | $81.7 \pm 44.4$ | $4.7 \pm 5.2$ | $6.9 \pm 3.5$ | 37 | |
| S. major (h5) | $63.2 \pm 44.1$ | $4.2 \pm 5.6$ | $6.4 \pm 3.0$ | 60 | $0.30 \pm 0.11$ |

of the velocities of the predator and the prey at the moment of the collision (23). A heuristic parameter estimation algorithm was used to determine the efficiency coefficients $(\lambda_A, \lambda_B, \xi_A, \xi_B)$, and the simulated predation rates closely matched the experimentally determined predation rates for all three strains of predatory *K. veneficum*.

### 4.1 Summary of prior experimental studies

In addition to observing that some strains of the mixotrophic dinoflagellate *K. veneficum* release karlotoxins to immobilize their prey and enhance predation, Sheng et al. also observed that the toxic strains of *K. veneficum* dramatically altered their swimming behavior when they were introduced to prey [27]. Using digital holographic microscopy, they were able to characterize the swimming properties of the various dinoflagellates $(\mathbf{v}, r, \omega)$, as well as their immotility $(\chi)$ and the time-averaged predation rate $\gamma$. Immotility $(\chi)$ is defined as the percentage of dinoflaggelates that are immobilized, and the time-averaged predation rate $(\gamma)$ is defined as the number of prey that disappeared per predator per hour. The experiments were conducted with four strains of *K. veneficum* (MD5, 1974, BM1, and 2064), with MD5 serving as a control due its nontoxic (and nonpredatory) nature. The cryptophyte *S. major* was used as prey during the experiments. The swimming properties were observed prior to mixing (control), immediately after mixing (h0), and 5 hours after mixing (h5). A summary of the experimental results from their study is shown in Table 2.

Several interesting observations can be made from the experimental data. The nontoxic (and nonpredatory) *K. veneficum* MD5 dinoflagellates did not change their swimming behavior when *S. major* was introduced to their environment, and the cryptophyte prey *S. major* did not change their swimming behavior either. Conversely, the toxic strains of *K. veneficum* altered their swimming behavior dramatically when *S. major* was introduced to their environment. The proportion of immotile cells

**Table 3.** Predatory efficiency coefficients. The standard deviations are included since the genetic algorithm used for the parameter estimation was run multiple times to compensate for its heuristic nature. The standard deviations are small relative to the mean values of the parameter estimates, which indicates that the algorithm successfully reached convergence.

| Coefficient | Value |
|---|---|
| $\lambda_A$ ($\mu$m/sec) | $152 \pm 20$ |
| $\lambda_B$ ($\mu$m/sec) | $20 \pm 2$ |
| $\xi_A$ | $3.0 \pm 0.1$ |
| $\xi_B$ | $25.5 \pm 4.1$ |

**Table 4.** Predation rate comparisons. Note that $k$ now represents the encounter rate and not the predation rate, since predation inefficiencies are being considered.

| *K. veneficum* Strain | Experimental $\gamma$ (1/hr) | Simulated $\gamma$ (1/hr) | Simulated $k$ ($m^3$/sec) |
|---|---|---|---|
| 1974 (toxic) | $0.39 \pm 0.13$ | 0.39 | $2.87 \times 10^{-14}$ |
| 1974 (control) | | 0.31 | $2.98 \times 10^{-14}$ |
| BM1 (toxic) | $0.36 \pm 0.06$ | 0.36 | $2.16 \times 10^{-14}$ |
| BM1 (control) | | 0.21 | $3.35 \times 10^{-14}$ |
| 2064 (toxic) | $0.30 \pm 0.11$ | 0.30 | $1.65 \times 10^{-14}$ |
| 2064 (control) | | 0.27 | $2.73 \times 10^{-14}$ |

increased for all three toxic strains upon introduction of prey, and *K. veneficum* BM1 and 2064 immediately experienced a sharp decrease in speed, while the average speed of *K. veneficum* 1974 increased instead. Toxin cell quotas presented by Sheng et al. suggest that *K. veneficum* released toxins when they encountered prey (*S. major*), resulting in a large increase in the proportion of immotile cells and sharp reductions in prey velocity. The experimental results presented by Sheng et al. are consistent with toxin potency and agree with previous studies [27]. The predation rate determined for *K. veneficum* MD5 is not an actual predation rate, since *K. veneficum* MD5 is nonpredatory, but rather an indicator of noise in the measurements.

### 4.2 Simulations based on experimental studies

Using the experimental data from Table 2 as a reference point, 100 simulations were run for each of the three strains of toxic dinoflagellates using the same simulation guidelines outlined in Sects. 2.2 and 3.2. These simulations accounted for the distributed parameters and immotility fractions of the dinoflagellates and calculated predation inefficiencies as a function of the velocities of the predators and the prey at the moment of collisions (23). The simulations in Sects. 2.2 and 3.2 used parameter sets from the dinoflagellates in their controlled (un-mixed) environments. However, the goal of the simulations presented in this section was to account for all of the complexities involved in dinoflagellate predation, including toxin release, immotility, parameter distributions, and inefficient predation. Therefore, the parameters were selected from the experimental cases where the *K. veneficum* was mixed with *S. major*. A genetic algorithm [14,20,23] was used to perform the parameter estimation for the predation efficiency coefficients, which are shown in Table 3. The resulting predation rate comparisons can be seen in Table 4, with good agreement between the simulated and experimental values. The simulation results indicate that the speed of the prey at the time of collision is the primary factor for determining predation efficiency based on our model (23), as $\lambda_B \ll \lambda_A$ and $\xi_A \ll \xi_B$. This indicates that there

is a sharp dropoff in predation efficiency at relatively low prey speeds as opposed to a gradual decline in efficiency at relatively high predator speeds. This result is somewhat intuitive and suggests that the use of toxins primarily enhances the predatory efficiency of the toxic strains of *K. veneficum* by enabling them to slow down and immobilize their prey.

A further set of simulations were used to quantitatively verify whether the release of toxins provided a predatory advantage to the toxic strains of *K. veneficum*. Using the behavior of the non-toxic MD5 dinoflagellate as a reference, 3 sets of "control" simulations were run where the predator-prey parameters were matched to the parameters of the species when they were not interacting with each other. Using the efficiency parameters calculated from the first set of simulations (see Table 3), the predation rates for these interactions were calculated for comparison and are shown in Table 4. The encounter rate $k$ was also provided for comparison. These simulations show that the use of toxins increases the predation rates of the predatory dinoflagellates anywhere from 11% to 71% depending on the specific variation, despite a reduction in the encounter rates. These results suggest that toxins increase predation rates by increasing predation efficiency at the expense of lowering the interaction rates. The benefit gained by increasing efficiency appears to outweigh the decrease in collision events.

## 5 Conclusions and future work

In this paper, we have applied modeling principles from simple swimmers and chemical kinetics to understand predation in plankton species. Leveraging recent experimental techniques that can determine swimming velocities with great precision, we have developed mathematical models that provide insight into how predator and prey species interact at a detailed level. Furthermore, we can validate our theory through simulation. We are particularly interested in the role of predation efficiency and toxins which can be deployed by predators to slow prey. We have demonstrated quantitatively that lowering the swimming speed can paradoxically increase predation. The explanation is that under certain circumstances, fewer interactions can lead to a net gain in predation when the individual interactions are more likely to lead to predation.

We acknowledge the support of NSF grant DMS-1261591 for supporting the Graduate Student Mathematical Modeling Camp where this problem was introduced. We acknowledge the support of camp coordinator Prof. Schwendeman at Renssaeler Polytechnic Institute, and the rest of the student plankton team including Seth Cowall, John Cummings, Jennifer Karkoska, Tim Krumwiede, Brittany McCollom, Rashmi Murthy, Thao Nguyen and Yuzhou Qian. The camp was the incubator for the initial simulations and many exciting mathematical discussions. We are also grateful to Dr. Allen Place (University of Maryland Center for Environmental Science) for helpful discussions.

## References

1. J. Adolf, T. Bachvaroff, D. Krupatkina, H. Nonogaki, P. Brown, A. Lewitus, H. Harvey, A. Place, Afr. J. Mar. Sci. **28**, 415 (2006)
2. J.E. Adolf, T. Bachvaroff, A.R. Place, Harmful Algae **8**, 119 (2008)
3. R.A. Alberty, *Physical Chemistry* (John Wiley & Sons, 1983)
4. M.N. Breckels, E.C. Roberts, S.D. Archer, G. Malin, M. Steinke, J. Plankton Res. **33**, 629 (2010)
5. A. Calbet, M. Bertos, C. Fuentes-Grünewald, E. Alacid, R. Figueroa, B. Renom, E. Garcés, Harmful Algae **10**, 654 (2011)

6. S. Chakraborty, S. Bhattacharya, U. Feudel, J. Chattopadhyay, Ecolog. Complexity **11**, 144 (2012)
7. H.C. Crenshaw, Bull. Math. Biol. **55**, 197 (1993)
8. H.C. Crenshaw, Bull. Math. Biol. **55**, 231 (1993)
9. J.R. Deeds, A.R. Place, Afr. J. Mar. Sci. **28**, 421 (2006)
10. J.R. Deeds, R.E. Hoesch, A.R. Place, Aquatic Toxicol. **159**, 148 (2015)
11. M.L. Echevarria, G.V. Wolfe, S.L. Strom, A.R. Taylor, FEMS Microbiol. Ecol. **90**, 18 (2014)
12. T. Fenchel, Protist **152**, 329 (2001)
13. L.E. Fleming, B. Kirkpatrick, L.C. Backer, C.J. Walsh, K. Nierenberg, J. Clark, A. Reich, J. Hollenbeck, J. Benson, Y.S. Cheng, J. Naar, R. Pierce, A.J. Bourdelais, W.M. Abraham, G. Kirkpatrick, J. Zaias, A. Wanner, E. Mendes, S. Shalat, P. Hoagland, W. Stephan, J. Bean, S. Watkins, T. Clarke, M. Byrne, D.G. Baden, Harmful Algae **10**, 224 (2011)
14. D.E. Goldberg, *Genetic Algorithms in Search, Optimization and Machine Learning* (Addison Wesley, Boston, 1989)
15. J.D. Hackett, D.M. Anderson, D.L. Erdner, D. Bhattacharya, Exp. Amer. J. Botany **91**, 1523 (2004)
16. H.J. Jeong, Y. Du Yoo, J.S. Kim, T.H. Kim, J.H. Kim, N.S. Kang, W. Yih, J. Eukaryotic Microbiol. **51**, 563 (2004)
17. J.W. Kempton, A.J. Lewitus, J.R. Deeds, J.M. Law, A.R. Place, Harmful Algae **1**, 233 (2002)
18. J.H. Landsberg, Rev. Fisheries Sci. **10**, 113 (2002)
19. N.D. Lewis, M.N. Breckels, M. Steinke, E.A. Codling, Ecolog. Complexity **16**, 41 (2013)
20. B.L. Miller, D.E. Goldberg, Evolutionary Comput. **4**, 113 (1996)
21. A.R. Place, J. Adolf, T.R. Bachvaroff, H. Zhang, S. Lin, J. Phycol. **43** (2007)
22. A.R. Place, H.A. Bowers, T.R. Bachvaroff, J.E. Adolf, J.R. Deeds, J. Sheng, Harmful Algae **14**, 179 (2012)
23. S.S. Rao, *Engineering Optimization: Theory and Practice* (Wiley, Hoboken, 2009)
24. M.S. Roth, Frontiers Microbiol. **5**, 1 (2014)
25. C. Schmoker, S. Hernandez-Leon, A. Calbet, J. Plankton Res. **35**, 691 (2013)
26. J. Sheng, E. Malkiel, J. Katz, J. Adolf, R. Belas, A.R. Place, Proc. Nat. Acad. Sci. United States Amer. **104**, 512 (2007)
27. J. Sheng, E. Malkiel, J. Katz, J.E. Adolf, A.R. Place, Proc. Nat. Acad. Sci. United States Amer. **107**, 2082 (2010)
28. A. Skovgaard, S.A. Karpov, L. Guillou, The parasitic dinoflagellates Blastodinium spp. Inhabiting the gut of marine, Planktonic copepods: Morphology, ecology, and unrecognized species diversity (2012)
29. F.J.R. Taylor, M. Hoppenrath, J.F. Saldarriaga, Dinoflagellate diversity and distribution (2008)
30. P. Tester, R. Waggett, A. Place, J. Phycol. **43**, 30 (2007)
31. F.M. Van Dolah, Environ. Health Perspectives **108**, 133 (2000)
32. R.M. Van Wagoner, J.R. Deeds, M. Satake, A.A. Ribeiro, A.R. Place, J.L.C. Wright, Tetrahedron Lett. **49**, 6457 (2008)
33. R.M. Van Wagoner , J.R. Deeds, A.O. Tatters, J. Nat. Prod. **73**, 1360 (2010)
34. R.J. Waggett, P.A. Tester, A.R. Place, Mar. Ecol.-Progress Ser. **366**, 31 (2008)
35. Y.D. Yoo, H.J. Jeong, M.S. Kim, N.S. Kang, J.Y. Song, W. Shin, K.Y. Kim, K. Lee, J. Eukaryotic Microbiol. **56**, 413 (2009)